NASA TECHNICAL MEMORANDUM

NASA TM-78846

NASA TM-78846

CORRELATION OF FIBER COMPOSITE TENSILE STRENGTH WITH THE ULTRASONIC STRESS WAVE FACTOR

by Alex Vary and Raymond F. Lark
Lewis Research Center
Cleveland, Ohio 44135

TECHNICAL PAPER to be presented at the
1978 Spring Conference
sponsored by the American Society for Nondestructive Testing
New Orleans, Louisiana, April 3-7, 1978

CORRELATION OF FIBER COMPOSITE TENSILE STRENGTH WITH THE ULTRASONIC STRESS WAVE FACTOR

by Alex Vary and Raymond F. Lark

National Aeronautics and Space Administration
Lewis Research Center
Cleveland, Ohio 44135

ABSTRACT

An ultrasonic-acoustic technique was used to indicate the strength variations of tensile specimens of a graphite-epoxy composite. A "stress wave factor" was determined and its value was found to depend on variations of the fiber-resin bonding as well as fiber orientation. The fiber orientations studied were 0° (longitudinal), 10° (off-axis), 90° (transverse), [0°/±45°/0°] symmetrical, and [±45°] symmetrical. The stress wave factor can indicate variations of the tensile and shear strengths of composite materials. The stress wave factor was also found to be sensitive to strength variations associated with microporosity and differences in fiber-resin ratio.

SUMMARY

A series of graphite fiber reinforced epoxy matrix (AS/PR-288) composite specimens were evaluated nondestructively. An ultrasonic-acoustic method was used to rank the specimens according to strength variations. The method used for this purpose involved the determination of stress wave propagation in the material (parallel to the tensile load axis). This measurement yielded a number termed the "stress wave factor". This factor is proportional to the stress wave energy transmitted by the material.

The primary variable in the series was fiber orientation. Five fiber orientations were used. These were 0° (longitudinal), 10° (off-axis), 90° (transverse), [0°/±45°/0°] symmetrical, and [±45°] symmetrical. A secondary variable was fiber-resin bonding which was altered by coating the fibers with polyvinyl alcohol (PVA). The specimens were designed for tensile testing and comparison of ultimate strength properties.

The most significant finding of this study was that the stress wave factor correlates strongly with ultimate tensile and shear strengths that accompany different fiber orientations and fiber-resin matrix bonds. Correlations that were obtained probably arose because stress wave propagation is a function of material stiffness which in turn controls ultimate strength in the composites tested. Also, by making equally-

spaced measurements along the specimen axis, it was possible to predict where fracturing would occur. None of the specimens contained intentional defects. Fracture apparently initiated at loci that were weakest because of microstructural variations rather than overt defects. The locations of the lowest stress wave factor values coincided with the locations of actual fractures.

INTRODUCTION

This report covers one of a series of studies concerned with nondestructive evaluation (NDE) of material strength properties of fiber-reinforced composites. This is part of an effort to investigate NDE techniques that will be suitable for ranking composite structures according to strength. The techniques would be applicable to verify inherent strength after other NDE tests have demonstrated that no overt defects, such as delaminations, exist in a given structure. The techniques should also apply to measuring strength degradation following exposure to operational environments.

In a previous study, it was demonstrated that the interlaminar shear strength of fiber reinforced composites can be indirectly measured by an ultrasonic-acoustic technique (ref. 1). In the aforementioned study a "stress wave factor" was determined for a series of composite specimens and the value of this factor was compared with the short beam shear strengths of the same specimens. Higher values of the stress wave factor corresponded to greater interlaminar shear strength.

In the previous study, the short beam shear test proved to be a sensitive indicator of material shear strength. The specimens were unidirectional and the principal variables were fiber fraction and micro-void content. For the study reported herein, a new set of specimens was designed for tensile testing. In these new specimens fiber orientation was the primary variable and fiber-resin bonding was a secondary variable. The objective was to find whether the stress wave factor was sufficiently sensitive to these two variables and hence accompanying strength variations.

SYMBOLS

[Basic SI dimensions appear in brackets.]

a	experimentally determined coefficient
b	experimentally determined exponent
E	tensile modulus, GPa, [$N\ m^{-2}$]

ε	stress wave factor
f_f	fiber weight fraction
g	time interval
k_v	porosity volume fraction
N_{sw}	normalized stress wave factor = $\varepsilon/\varepsilon_{max}$
n	number of oscillations exceeding a threshold
r	repetition rate of stress wave bursts
t	specimen thickness, cm, [m]
ν	Poisson's ratio
ρ_c	composite density, g cm^{-3}, [kg m^{-3}]
σ_{ut}	ultimate strength, GPa, [N m^{-2}]

EXPERIMENTAL PROCEDURE AND RESULTS

Specimens

A number of 8-ply panel laminates were made using a standard method of fabrication and curing. The fabrication procedure is described in Appendix A. Only the fiber orientation and fiber-resin bonding were intentionally varied in the panels. The fiber orientation scheme is depicted in figure 1. After the panels were completed and inspected for defects, each one was cut into a number of strips to serve as tensile specimens. Physical details of the specimens are given in table I. The specimen designs included a variety of fiber orientations that would lead to different ultimate strengths, moduli, and fracture modes. The anticipated fracture modes included fiber tearing, intralaminar shear, interlaminar shear, and matrix failure.

Nondestructive Evaluations

Prior to being cut into specimens each panel was examined for defects using an immersion ultrasonic scanning method. The procedure used is described in reference 1. The ultrasonic scanning inspections indicated that there were no serious flaws in the panels. However, there were local inhomogeneities in fiber distribution and indications that the fiber/resin ratio varied slightly. The small variations that

did exist were considered fortuitous because they would furnish data on the effect of local inhomogeneities.

Once the strips were cut from the panels, each one was subjected to measurements of the "stress wave factor". Fifteen equally-spaced overlapping measurements were made along the length of each strip. The transducer probe arrangement for making these measurements is indicated in figure 2 and the method is described in Appendix B. From the data obtained it was possible to assign a value for the stress wave factor at regular intervals along the length of the strips. Axial variations of the stress wave factor could thus be plotted in order to locate microstructural anomalies (weak areas) in the test zone.

Tensile Failure Modes

The tensile testing instrumentation and loading are described in Appendix C. All specimens failed in a brittle fracture mode and always within the gage length. As detailed in Appendix D, intralaminar shear, interlaminar shear, matrix fracture, and fiber tearing were evident to various degrees in these specimens according to the fiber orientation. Fracture modes are summarized in table II and illustrated in figure 3.

Strength and Moduli

Results of the tensile tests are given in table III. The tensile test instrumentation data were reduced with the Lewis Research Center SGDR (Strain Gage Data Reduction) computer program, reference 2. For the ultimate axial (tensile) strengths, σ_{11t}, the average test section thickness and width for each specimen was used to calculate the cross sectional area. For the six 10-degree off-axis specimens, the ultimate intralaminar shear strength was calculated, reference 3. The strengths, moduli, strength/modulus (σ_{ut}^2/E), and Poisson's ratios given in table III are based on the average of paired back-to-back strain gage readings for each specimen. Manufacturer's strength and modulus values are also given in table III for the graphite fiber and neat resin.

Failure Loci

Figure 4 shows plots of the variation of the stress wave factor vs. linear distance along representative specimens. Plots for only three typical cases out of twenty-seven specimens are shown in figure 4. The relative sensitivity of the stress wave factor measurements is indicated by the ordinate scale. Overall sensitivity was about ± 2 percent of full scale. As mentioned in Appendix B, ε was measured at 15 stations along each specimen prior to attachment of the tabs. After the specimens failed under tensile loading, the separate pieces were

reassembled and the fracture loci were noted. A scale drawing of the corresponding specimen accompanies each graph in figure 4. The location where the specimen failed is indicated in each case. It is apparent that the failures occurred at minimum ε values. In the case of multiple fractures, there were several correspondingly low ε values. It is noteworthy that these fracture loci gave no indications of overt defects such as delaminations in prior ultrasonic inspections. Thus, flaws, if present, were so minute or diffuse that they were sensed only as decreases in the ε values.

Strength Correlations

Figure 5(a) shows plots of strengths of the PVA-treated specimens (LV11, LV22, and LV33) against corresponding non-PVA treated specimens (LV1, LV2, and LV3). For the 0° (longitudinal) and [0°/±45°/0°] symmetrical specimens the PVA coating apparently lowered the ultimate strength, as expected. For the 90° transverse specimens, however, the PVA specimens (LV22) exhibited higher strengths. Since the fiber fractions were approximately equal for LV2 and LV22 specimens, the strength difference can be attributed to the roughly 3 to 1 ratio in mean void content, see table I. Thus, the PVA specimens (LV22) had higher strength because of lower void content than the non-PVA specimens (LV2). The strength properties of the other specimens were probably not as strongly influenced by void content. The results shown in figure 5(a) indicate that only the 90° (transverse) specimen strengths were inverted relative to the equivalence line by the unintentional voids introduced during fabrication.

Figure 5(b) shows a plot of the normalized stress wave factor N_{sw} as a function of ultimate strength. The plot indicates a monotonic increase of N_{sw} with σ_{ut}. The regression curve fitted to the data has a coefficient of determination of 0.996. Increases in the stress wave factor correspond to increases in ultimate tensile strength. Thus, figure 5(b) demonstrates that the stress wave factor correctly ranked ultimate strengths despite porosity variations and the inversion noted in figure 5(a). Note that in figure 5(b) the neat resin falls outside the standard deviation bounds and the strength of the neat resin is equivalent to that of the (LV2) 90° transverse specimens but at a higher value of N_{sw}. This is expected since the neat resin has no fibers to impede wave propagation.

Figure 5(c) shows N_{sw} as a function of σ_{ut}^2/E. This latter quantity is a measure of strain energy at ultimate load (i.e., if x is gage length, then $\sigma_{ut}^2 x/Ex$ has the dimensions of energy per unit volume, MJ/m^3). Since, as indicated in DISCUSSION, N_{sw} is also related to energy (stress wave energy), it is appropriate to plot N_{sw} vs. σ_{ut}^2/E. By consulting the fiber fraction data in table I it is found that those specimens with the lowest fiber fraction are slightly below

the fitted curve and those with the highest fiber fraction are slightly above it. By plotting N_{sw}/f_f vs. σ_{ut}^2/E as in figure 5(d) we obtain a better curve fit with less scatter. In figure 5(d) the coefficient of determination is 0.987 vs. 0.972 for figure 5(c). This indicates higher sensitivity of N_{sw} to relatively small variations of fiber fraction in comparison to the strength-modulus ratio. This is readily seen by regression analysis of the data for figure 5(d) from which we obtain the equation,

$$N_{sw} = af_f \left(\sigma_{ut}^2/E\right)^b$$

where regression analysis gives a = 0.6560 and b = 0.2376. Thus, it is seen that N_{sw} varies with the first power of f_f and with only a fractional power of σ_{ut}^2/E.

Figure 5(e) shows the effect of specimen thickness by a plot of $N_{sw}t/f_f$ vs. σ_{ut}^2/E. Note that we now get two curves: one for PVA, the other for non-PVA specimens (each having a goodness of fit of 0.995). It was found that the PVA coating added approximately 9.2 micrometers to the original diameter of the fiber. This is approximately 5 percent over the original fiber diameter of 180 micrometers. From figure 5(e) it is clear that both N_{sw} and σ_{ut}^2/E are sensitive to this difference in microstructure. However, increased thickness or fiber diameter is not the sole effect of the PVA fiber coating. As indicated with reference to figure 5(a), an interplay among the PVA, void content, and fiber fraction contributed to the net strengths.

DISCUSSION

The stress wave factor N_{sw} may be described as a measure of the efficiency of stress wave energy transmission. The working hypothesis was that decreased stress wave energy flow corresponds to decreased fracture resistance. The findings given herein and previously reported results (ref. 1) appear to support this view.

The stress wave factor provides a means of rating the efficiency of dynamic strain energy transfer in a given composite. Our view of the results given herein is that a material which is more efficient in transfer of stress wave energy will exhibit greater strength. That is, better stress wave transmission means better transmission of dynamic stress and load distribution. Conversely, low values of N_{sw} would indicate places where dynamic strain energy is likely to concentrate and promote fracture.

The nature of the actual tensile failures confirmed the above premise. The 0° unidirectional specimens (LV1 and LV11 had the highest N_{sw} values and highest ultimate tensile strengths. These specimens failed "explosively" and fractured at numerous locations in the gage zone (see fig. 3 and Appendix D). This can be interpreted as indicating efficient transmission and distribution of dynamic stress energy. Specimens with $\pm 45°$ plys alternating with 0° plys (LV3 and LV33) had the next lowest N_{sw} values and strengths. Moreover, this latter group of specimens typically failed only at locations with the lowest N_{sw} values. It appears, therefore, that fiber orientation is critical not only to sustaining static loading but also to dynamic stress wave transmission, references 4 and 5.

The stress wave factor value generated for each test area depends on the wave propagation direction relative to the fibers. Other factors that influence the magnitude of the value are fiber bonding, fiber-resin ratio, microvoids, interlaminar bonding, etc. The number generated is a purely relative one that will differ for substantially different specimen geometries, fiber orientations, widths, thicknesses, materials, etc. It is probable that the correlations obtained arise because stress wave propagation is a function of material stiffness which in turn governs strength.

SUMMARY OF RESULTS AND CONCLUSIONS

It has been shown that ultrasonic-acoustic wave propagation properties of a fiber reinforced composite are significant indicators of mechanical properties such as ultimate tensile and shear strengths. An approach was described for measuring a quantity termed the "stress wave factor". This quantity was measured nondestructively and compared with destructive test measurements of tensile properties of specimens of the composite AS/PR-288, a graphite reinforced epoxy. Major results and conclusions that may be drawn from the work described herein are:

1. The stress wave factor is a sensitive indicator of composite strength variations that accompany various fiber orientations relative to the load axis.

2. For a given fiber orientation the stress wave factor is also sensitive to strength variations associated with differences in fiber-resin bonding, voids, and fiber-resin ratios.

3. For the composite tensile specimens studied, the stress wave factor decreased proportionally with fractional powers of ultimate strength.

4. The stress wave factor may be a useful aid in predicting potential failure locations in thin composite laminates.

APPENDIX A

SPECIMEN FABRICATION

The fiber-resin system selected for this study consisted of type AS graphite fiber and PR-288 epoxy resin. Eight 8-ply panel laminates were made as indicated in table I and figure 1. Each ply originated as AS/PR-288 prepreg tape. The starting material was AS-1 Hercules fiber tow with 10,000 filaments per tow.

Two different treatments were used on the fibers: one batch of tape was made from fibers treated with PVA (polyvinyl alcohol) while another batch of tape was made without PVA coating on the fiber. For the non-PVA specimens the tape was made directly from fibers impregnated with an amount of resin that would yield a cured ply thickness of about 0.13 mm (0.005 in) and between 65 and 75 percent fiber weight fraction. Density of the fiber was approximately 1.80 g/cc and density of the resin was approximately 1.27 g/cc. For the PVA specimens the fibers were first coated with PVA and then formed into resin impregnated tape.

The prepreg tapes were 7.6 cm (3 in) wide. They were fitted into a mold that was 15.3 cm (6 in) wide by 30.5 cm (12 in) long to form the fiber orientations indicated in table I. After stacking 8 plys, the material in the mold was placed in a hydrostatic press with platens heated to 177 °C (350 °F) and held under contact pressure until the material reached 37.7 °C (100 °F). The pressure was raised to 2.07 MPa (300 psi) in approximately 30 seconds. This cure pressure was then held for 2 hours at 177 °C (350 °F).

After curing, the panel laminates were removed from the mold while still hot and allowed to cool to room temperature. Each panel was then ultrasonically scanned for defects. After this ultrasonic inspection, selected portions of the panels were cut into strips having the dimensions indicated in table I. Cutting was done with a water-cooled diamond wheel. In addition to the strips destined for tensile testing, small coupons were extracted from the panels for the density and fiber weight fraction determinations given in table I.

Each strip was subjected to measurement of the stress wave factor as explained in Appendix B. Following these measurements, aluminum tabs were bonded to the ends of each strip. These tabbed strips constituted the tensile specimens used in this study. The tabs were 6.3 cm (2.5 in) long resulting in the gage lengths listed in table I. It should be noted that in order to bond tabs to the specimens, an additional thermal cycle had to be used to cure the adhesive. This amounted to a post cure of the composite at 177 °C (350 °F) for 2 hours.

Each specimen was inscribed with an identification and also a fiducial mark. The fiducial was a reference for proper orientation when locating stress wave factor measurements relative to fracture loci after tensile testing.

APPENDIX B

STRESS WAVE SIMULATION MEASUREMENTS

The method described herewith is applied to one area at a time, and it generates a number associated with that area. The probes are positioned axially along the specimen. Fifteen equally spaced, overlapping measurements were made. Fifteen "stress wave factor" numbers were thus generated for each tensile specimen. (The time taken to make these 15 readings is approximately 0.5 minutes per specimen.)

A sending transducer injects a repeating series of ultrasonic pulses into the material. Each of these pulses produces simulated stress waves that mimic acoustic emission events in the material, references 6, 7. A receiving transducer intercepts some of the simulated stress wave energy that radiates from the point of injection.

The transducer configuration for simulation of stress waves and measurement of the stress wave factor is illustrated in figure 2. Stress wave simulation was accomplished with a 2.25 MHz piezoelectric transducer coupled directly to the specimen surface. The receiving transducer was a piezoelectric acoustic emission transducer having a resonant frequency of approximately 0.5 MHz and an effective bandwidth of roughly 1 MHz. The sending transducer had a 0.63 cm (0.25 in) diameter crystal. The solid pick-up cone on the receiver waveguide was 1.27 cm (0.50 in) in diameter. Water with a wetting agent was used as a couplant.

The sending transducer injects longitudinal waves into the specimen. In the zone of injection mode conversion effects occur. The waves emanating from this zone are therefore complex and have both transverse as well as longitudinal components. The receiver is coupled to the surface through a waveguide. The waveguide effectively transmits only the longitudinal component of the wave that is coupled into it. The waveguide also serves as a delay line that separates the received signal from the input pulse for analytical purposes.

The signals arriving at the receiver resemble "burst" type acoustic emission events (ref. 8). After traveling through the composite, these simulated stress waves bear the imprints of factors that might alter an actual stress wave emanating from the injection zone. The simulated stress waves are repeated at a fixed rate r. The received signal roughly resembles a decaying sinusoid. Each successive "burst" is identical to its predecessors. After amplification, the received signals are sent to a counter that counts the number of oscillations n in each burst exceeding a fixed threshold voltage. The counter is reset automatically after a predetermined time interval

g and the previous count is held in a memory and digitally displayed. The displayed count assumes a constant value soon after the specimen is coupled to the probes. The number that is displayed is $\varepsilon = grn$, the stress wave factor. The stress wave factor appearing in table III, N_{sw}, is normalized relative to the maximum value found for ε found for all specimens, i.e., $N_{sw} = \varepsilon/\varepsilon_{max}$.

The number N_{sw} depends on factors such as probe pressure, coupling, signal gain, reset time, threshold voltage, repetition rate, and so forth. All these factors are, however, kept constant for any series of measurements so that N_{sw} reflects only the material variations of the specimens tested. Frequency spectrum analyses reveal prominent resonance peaks in the simulated stress wave signal. The peaks occur at similar frequencies regardless of fiber orientation. These are attributable to wave resonances associated with the specimen thickness. Prior studies (refs. 6,9) have shown that thin materials will exhibit thickness resonances. The stress wave factor was influenced by multiple reverberations in the thin specimens of this report. The signal sensed by the receiving transducer was thus generally a function of plate thickness as well as material property variables.

APPENDIX C

TENSILE TEST INSTRUMENTATION AND LOADING

The tabbed specimens were mounted in a tensile machine with self-adjusting vise grips. Serrations in these grips bit into the soft aluminum tabs upon loading. Care was taken to align the specimens to avoid off-axis loading or twisting. Initial loading was done at a rate of approximately 20 μm/s (0.04 in/min) to set the grips. After this initial loading to about 445 N (100 lbf), further loading was done at a mean rate of approximately 4 μm/s (0.01 in/min).

The loading was halted periodically at from 445 N to 1330 N (100 lbf to 300 lbf) increments for recording of strain gage data. Strain gages were attached to both sides of each specimen, i.e., paired, back-to-back at the center of the gage section. The (LV4) 10° off-axis specimens were instrumented with back-to-back 60° delta rosettes, see reference 2. All the other specimens were instrumented with orthogonal (0° and 90°) back-to-back strain gage pairs.

Because of material relaxation and tab creep effects, the loading rate was not reduced to zero during the "halts". To maintain a constant load during the halts, it was necessary to adjust the loading rate to slightly greater than zero.

APPENDIX D

FRACTURE MODES

The most dramatic failure occurred with the 0° unidirectional LV1 and LV11 specimens. All of these invariably fractured in several places. They fractured rather "explosively", splintering and making it hard to recover pieces thrown off. There was considerable intralaminar shear failure in the axial direction, parallel with the fibers, in the six specimens of this group, see figure 3. This matrix shear failure occurred in addition to the tensile failure by fiber tearing. This latter failure mode always occurred in a line that was perpendicular to the tensile axis.

The LV2 and LV22 (90°) transverse unidirectional specimens exhibited clean fractures in the resin matrix, parallel with the fibers. Thus, all fractures in the six specimens involved were on a line perpendicular to the tensile axis. No fiber tearing was evident.

The LV3 and LV33 specimens had alternating 0° and $\pm$45° plys. The fracture zones exhibited mainly fiber tearing accompanied by slight intra- and interlaminar shear failure. In all six cases, fractures were on a line that was perpendicular to the tensile axis.

The LV4 specimens failed in intralaminar shear, parallel with the 10-degree off-axis unidirectional fibers. The fracture surface was essentially a clean break in the resin matrix, although a small amount of fiber tearing occurred at the point seen in figure 3 in a few LV4 specimens. It is uncertain whether this tearing preceded or followed the matrix intralaminar shear failures in the specimens involved.

The LV55 specimens had only $\pm$45° plys. These specimens failed in interlaminar shear with accompanying fiber tearing and intralaminar separations. All fractures edges were at angles of either +45° or -45° relative to the tensile axis.

REFERENCES

1. A. Vary and K. J. Bowles. "Ultrasonic Evaluation of the Strength of Unidirectional Graphite-Polyimide Composites," NASA TM X-73646, 1977.

2. C. C. Chamis, J. Kring, and T. L. Sullivan, "Automatic Testing Data Reduction Computer Program," NASA TM X-68050, 1972.

3. C. C. Chamis and J. H. Sinclair, "10-Degree Off-Axis Tensile Test for Interlaminar Shear Characterization of Fiber Composites," NASA TN D-8215, 1976.

4. D. R. Curran, L. Seaman, and D. A. Shockey, Phys. Today, Vol. 30, (1977) p 46.

5. F. C. Moon, "A Critical Survey of Wave Propagation and Impact in Composite Materials," NASA CR-121226, May 1973.

6. D. M. Egle and A. E. Brown, J. Acoust. Soc. Am., Vol. 57, (1975), p 591.

7. D. M. Egle and A. E. Brown, J. Test. Eval., Vol. 4, (1976), p 196.

8. L. J. Graham and G. A. Alers, Monitoring Structural Integrity by Acoustic Emission, ASTM Special Technical Publication 571, Philadelphia, Pa., (1975), p 11.

9. A. Vary and K. J. Bowles, "Use of Ultrasonic-Acoustic Techniques for Nondestructive Evaluation of Fiber Composite Strength," in Proc. of the 33rd Annual Conference of the Society of the Plastics Industry, Washington, D.C., Feb. 1978, NASA TM-73813, 1978.

TABLE I. - DESCRIPTION OF GRAPHITE-EPOXY TENSILE SPECIMENS[a]

Specimen	Number tested	Ply[b] angle, deg	Fiber[c] coating	Gage length, cm	Thickness[d] t, cm	Density[e] ρ_c g/cm^3	Fiber[f] fraction %, f_f	Porosity[g] volume %, k_v
LV1	3	$[0]_8$	none	12.7	0.1024	1.572	65.7	0.05
LV11	3	$[0]_8$	PVA	12.7	0.1384	1.584	69.2	0.03
LV2	3	$[90]_8$	none	12.7	0.0981	1.588	74.2	0.10
LV22	3	$[90]_8$	PVA	12.7	0.1329	1.603	74.6	0.03
LV3	3	$[0/\pm45/0]_s$	none	12.7	0.1002	1.581	70.5	0.10
LV33	3	$[0/\pm45/0]_s$	PVA	12.7	0.1355	1.598	72.8	0.04
LV4	6	$[10]_8$	none	17.8	0.1042	1.611	69.6	0.07
LV55	3	$[\pm45]_s$	PVA	12.7	0.1340	1.599	71.7	0.06

[a]AS-1 graphite fibers in PR-288 epoxy matrix.

[b]Angle relative to tensile axis, see figure 1.

[c]PVA = polyvinyl alcohol, see Appendix A.

[d]Average for gage length, width was 1.27±0.002 cm.

[e]Fiber density = 1.78 to 1.81 g/cm^3, resin density ≅ 1.27 g/cm^3.

[f]Fiber weight fraction determined by HNO_3 digestion (ASTM-D3171).

[g]Porosity volume fraction by oil ingestion method (ASTM-B328).

TABLE II. - FRACTURE MODES OF GRAPHITE-EPOXY SPECIMENS[a]

Specimens	Fiber angles	Fracture modes
LV1 & LV11	0° (longitudinal)	Fiber tearing, fiber-matrix debonding with fiber pullout, intralaminar shear of matrix, tensile fracture of matrix
LV2 & LV22	90° (transverse)	Tensile fracture of matrix
LV3 & LV33	0°/±45°/0° (symmetrical)	Fiber tearing, fiber pullout, interlaminar shear failure, intralaminar matrix shear
LV4	10° (off-axis unidirectional)	Intralaminar shear fracture of matrix, (occasional tensile fracture of matrix and fiber tearing)
LV55	± 45° (symmetrical)	Fiber tearing, fiber fracture, interlaminar shear failure, intralaminar matrix shear

[a]AS-1 graphite fibers in PR-288 epoxy matrix. See Appendix D for additional descriptions of fracture modes, and figure 3 for illustrations of fractures.

TABLE III. - RESULTS OF DESTRUCTIVE AND NONDESTRUCTIVE TESTS

Specimen	Ply[a] angle	Fiber coating	Ultimate[b] strength σ_{ut}, GPa	Tensile[c] modulus E, GPa	Strength-[d] modulus, σ_{ut}^2/E, MPa	Poisson's[e] ratio, ν	Stress wave factor[f]	
							N_{sw}	N_{sw}/f_f
LV1	$[0]_8$	none	1.41	116	17.1	0.330	0.862	1.31
LV11	$[0]_8$	PVA	1.24	110	14.0	0.283	0.853	1.23
LV2	$[90]_8$	none	0.0584	10.2	0.334	0.0961	0.402	0.542
LV22	$[90]_8$	PVA	0.0672	8.27	0.546	0.0180	0.413	0.554
LV3	$[0/\pm45/0]_a$	none	0.807	73.9	8.81	0.615	0.755	1.07
LV33	$[0/\pm45/0]_s$	PVA	0.703	83.4	5.93	0.618	0.767	1.05
LV4	$[10]_8$	none	0.0800	7.41	0.867	0.487	0.424	0.609
LV55	$[\pm45]_s$	PVA	0.181	20.1	1.64	0.730	0.507	0.707
resin[g]	—	—	0.0579	3.45	0.973	—	0.518	—
fiber[h]	—	—	3.10	238	40.4	—	—	—

[a]Fiber angles relative to tensile axis in AS-graphite, PR-288 epoxy composite.

[b]Ultimate intralaminar shear stress is listed for 10° off-axis specimens (LV4). Ultimate tensile stress for the LV4 specimens = 0.469 GPa, computed on the basis of gage cross section area as for the other specimens.

[c]Moduli are calculated from initial slopes. Shear modulus is listed for LV4.

[d]Strength-modulus ratio for LV4 is based on shear strength and shear modulus.

[e]Poisson's ratios are based on initial slopes.

[f]$N_{sw} = \varepsilon/\varepsilon_{max}$, see Appendix B. Fiber weight fractions f_f are listed in table I.

[g]Strength and modulus are manufacturer's values for resin castings.

[h]Strength and modulus are manufacturer's values for 10,000 filament tows.

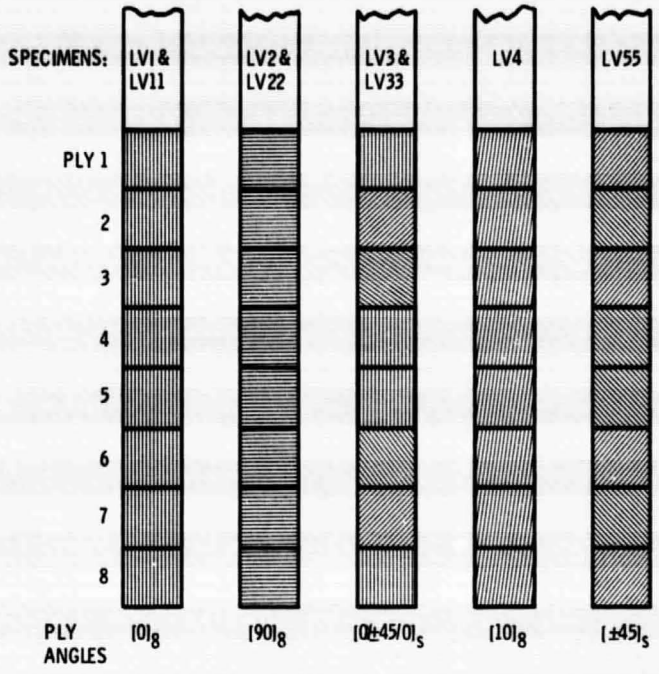

Figure 1. - Ply-by-ply fiber orientation scheme in graphite/epoxy composite specimens.

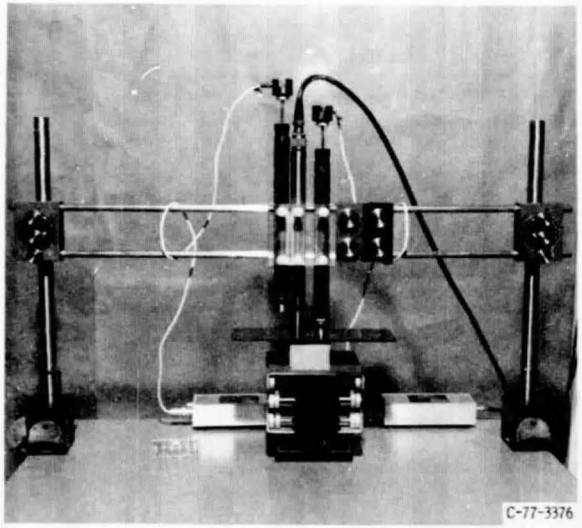

(a) DETAIL VIEW OF PROBES AND FIXTURE.

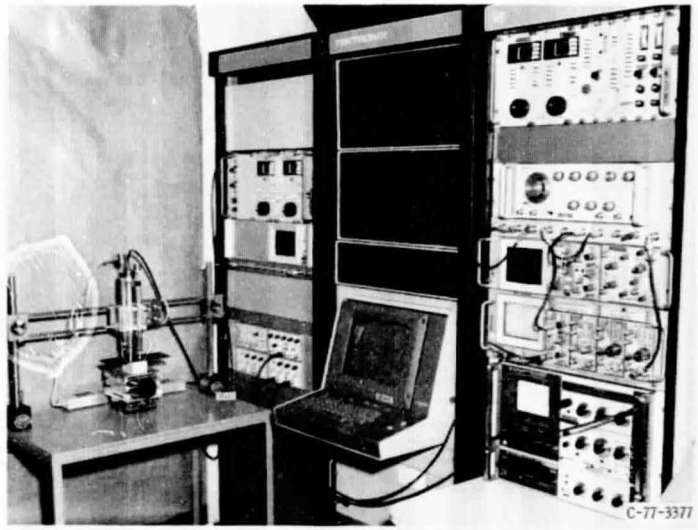

(b) OVERALL VIEW OF ULTRASONIC SYSTEM.

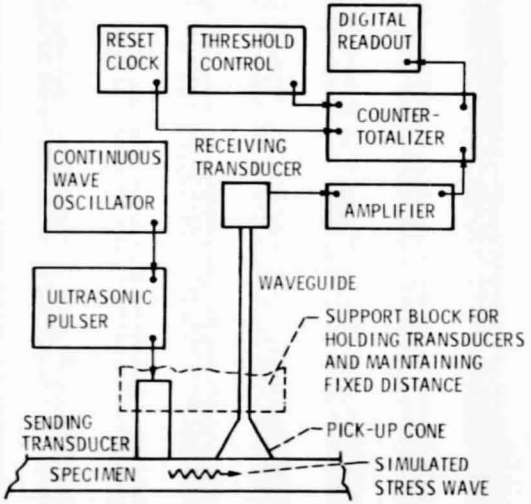

(a) APPARATUS FOR STRESS WAVE SIMULATION & MEASUREMENT.

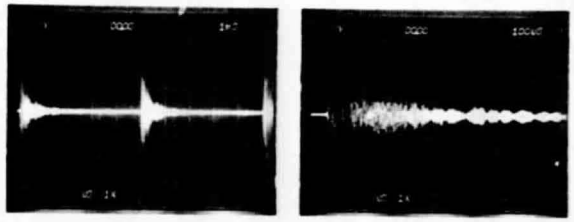

OSCILLOSCOPE TRACE SHOWING CONTINUOUSLY REPEATING BURSTS OF SIMULATED STRESS WAVES.

SINGLE BURST WAVEFORM. THRESHHOLD OF OSCILLATION COUNTS IS ± 0.5 SCALE DIVISION.

(d) SIGNALS USED FOR STRESS WAVE OSCILLATION COUNT.

Figure 2. - Apparatus and signal treatment used for measuring stress wave factor.

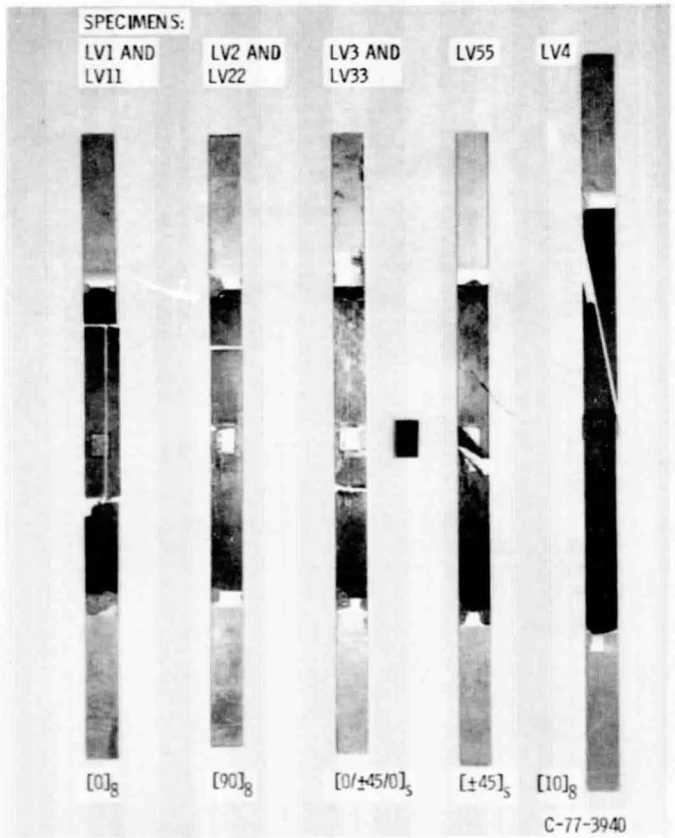

Figure 3. - Fractured graphite-epoxy tensile specimens exhibiting typical fracture modes associated with fiber angles indicated. (See table II).

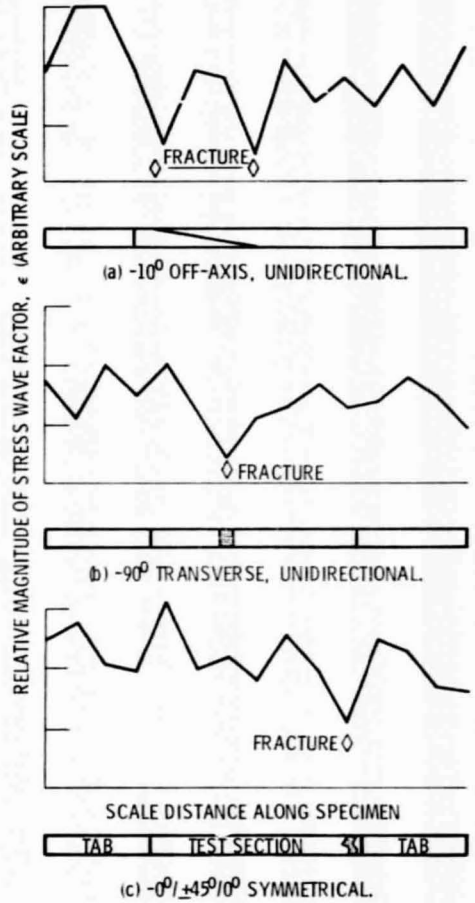

Figure 4. - Variation of stress wave factor along tensile specimen for three typical cases.

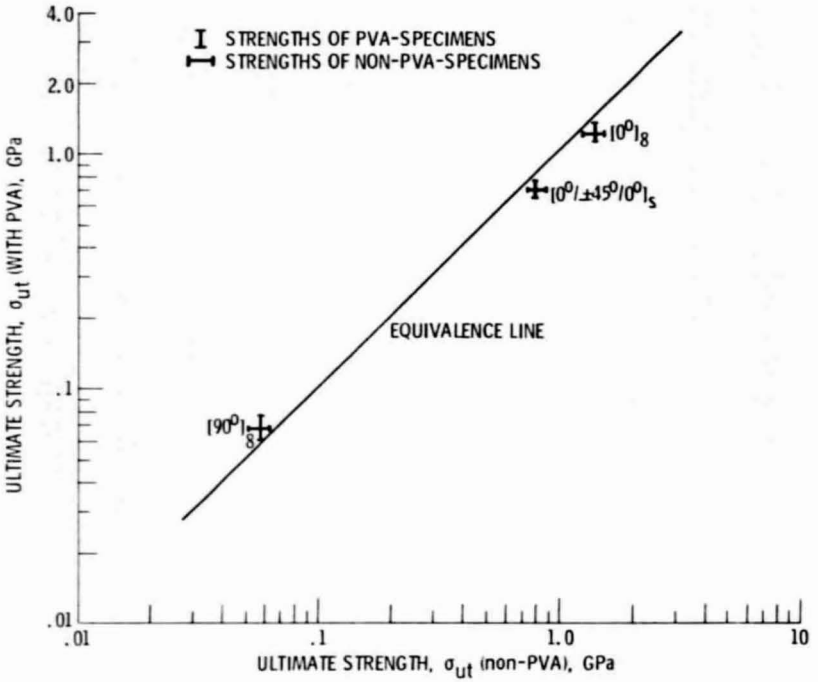

(a) ULTIMATE STRENGTH COMPARISON OF SPECIMENS WITH PVA-COATED FIBERS VS SPECIMENS WITH NON-PVA-COATED FIBERS (LV11, LV22, AND LV22 VS. LV1, LV2, AND LV3).

Figure 5. - Strength, modulus, and stress wave factor correlations for tensile specimens of the graphite-epoxy composite AS/PR-288.

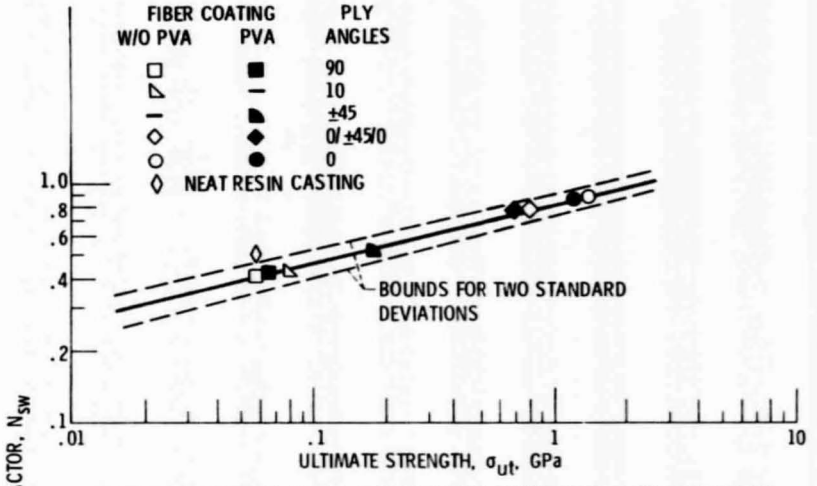

(b) STRESS WAVE FACTOR AS A FUNCTION OF ULTIMATE STRENGTH (COEFFICIENT OF DETERMINATION FOR FITTED CURVE IS 0.996).

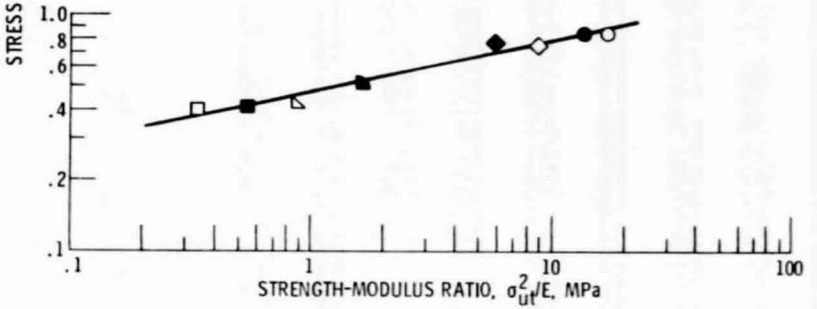

(c) STRESS WAVE FACTOR AS A FUNCTION OF STRENGTH-MODULUS RATIO (COEFFICIENT OF DETERMINATION FOR FITTED CURVE IS 0.972).

Figure 5. - Continued.

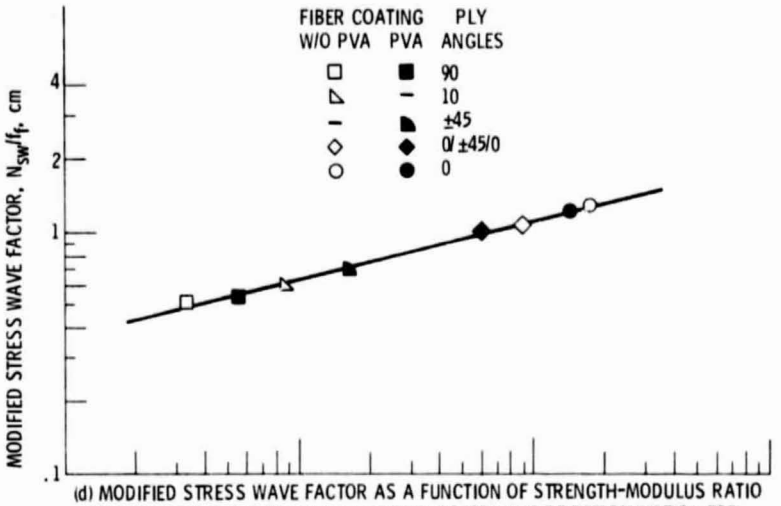

(d) MODIFIED STRESS WAVE FACTOR AS A FUNCTION OF STRENGTH-MODULUS RATIO SHOWING THE EFFECT OF FIBER FRACTION (COEFFICIENT OF DETERMINATION FOR FITTED CURVE IS 0.987).

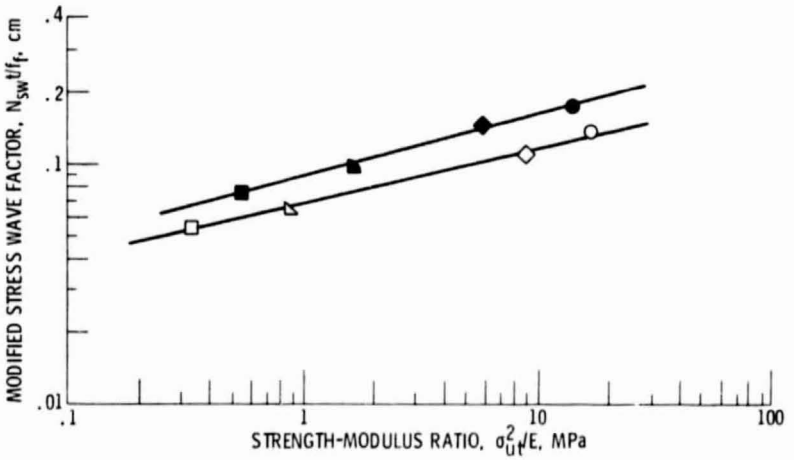

(e) MODIFIED STRESS WAVE FACTOR AS A FUNCTION OF STRENGTH-MODULUS RATIO SHOWING THE COMBINED EFFECTS OF FIBER FRACTION AND SPECIMEN THICKNESS (COEFFICIENT OF DETERMINATION FOR FITTED CURVES IS 0.995, EACH).

Figure 5. - Concluded.